CHAPTER 2

Experimental techniques and theoretical background

2.1 Introduction

This chapter describes the different experimental techniques used in the characterization of the physical and mesomorphic properties *viz.* birefringence (Δn), dielectric anisotropy ($\Delta\varepsilon$), splay elastic constant (K_{11}), figure of merit (FoM), relaxation time (τ_0), viscosity (bulk, rotational and effective torsional), spontaneous polarization (P_s), activation energy (E_a), layer spacing (d), tilt angle(θ), correlation length *etc.* of the liquid crystalline compounds and multi-component mixtures. An understanding of the working principle of these techniques and the behavior of the liquid crystalline materials under those experimental configurations has been discussed. The Maier–Saupe mean field theory [1–3] for the nematic phase has been illustrated briefly, since the experimentally determined orientational order parameter (S) have been compared with the theoretically predicted values. Moreover, a very concise description of the elastic continuum theory [4-7] and Freederiksz transition [8,9] has also been given in this chapter.

2.2 Experimental techniques

2.2.1 Texture studies

Texture studies by polarizing optical microscopy have been employed as a primary tool for the characterization and determination of the transition temperatures of the different liquid crystalline phases. The textures of different phases of liquid crystalline samples placed between crossed polarizer and analyzer, were observed using a polarizing optical microscope, Motic BA300 equipped with a Mettler Toledo FP90 thermo system [10,11]. Textures are generated due to the defects in structure that occurs in the long range molecular ordering of the liquid crystalline materials. Hence, defects in liquid crystals are important for the identification of different type of mesophases. The phase transitions could be observed clearly through the polarizing microscope when the

temperature of the sample is slowly varied. A detailed description of different textures with photographs is given by Demus [12] and Dierking [13].

2.2.2 Differential scanning calorimetry

Differential scanning calorimetry (DSC) has been used as a complementary tool to polarizing optical microscopy (POM). DSC measurement reveals the presence of liquid crystal phases by detecting the enthalpy change associated with the phase transitions. DSC is poor at detecting low enthalpy transitions such as second order. Although the calorimetry cannot identify the type of phases as POM, some useful information about the purity [14], order of the phase transition [15,16], conformational disorder [17] and molecular shapes can be derived from DSC. The phase transition temperatures were determined by differential scanning calorimetry using Pyris Diamond Perkin-Elmer 7 [18]. The sample (~ 6.97 mg) was hermetically sealed in an aluminium pan and placed in a nitrogen atmosphere within the sample chamber of the DSC instrument. The temperature and enthalpy change (ΔH) have been calibrated on extrapolated onsets of the melting points of ice, indium and zinc. Due to the ambiguity in defining the location of the transition temperatures by optical microscopy, several cooling or heating runs at the rate of $5^{o}Cmin^{-1}$ in a nitrogen atmosphere were performed. Determination of phase transition temperatures from DSC measurements have been discussed in the literature [19]. With the aid of computers, the transition temperatures and enthalpy change can be easily derived from the peaks and corresponding area of the DSC scans respectively.

2.2.3 X-ray diffraction study

The structural properties of the liquid crystalline compounds can be studied conveniently from x-ray diffraction studies. Vainshtein [20] and Leadbetter [21,22] have given the theoretical interpretation for the x-ray diffraction of liquid crystals. From this measurement, information on both the intermolecular and intra-molecular arrangement in the liquid crystals can be retrieved.

The x-ray diffraction pattern appears as an arc and this can be interpreted in terms of the orientational distribution of the ordered liquid crystal molecules [23,24]. X-ray diffraction of the un-aligned nematic phase consists of a uniform halo just like that of an isotropic liquid (Figure 2.1(a)). This is due to the fact that a nematic liquid crystal generally consists of a large number of domains, the molecules being ordered within each domain along the director **n**, but there is no preferred direction for the sample as a whole so that the diffraction pattern has symmetry of revolution around the direction of the x-ray beam. However, application of suitable magnetic or electric field can produce a 'monodomain' or 'aligned' or 'oriented' sample of liquid crystal.

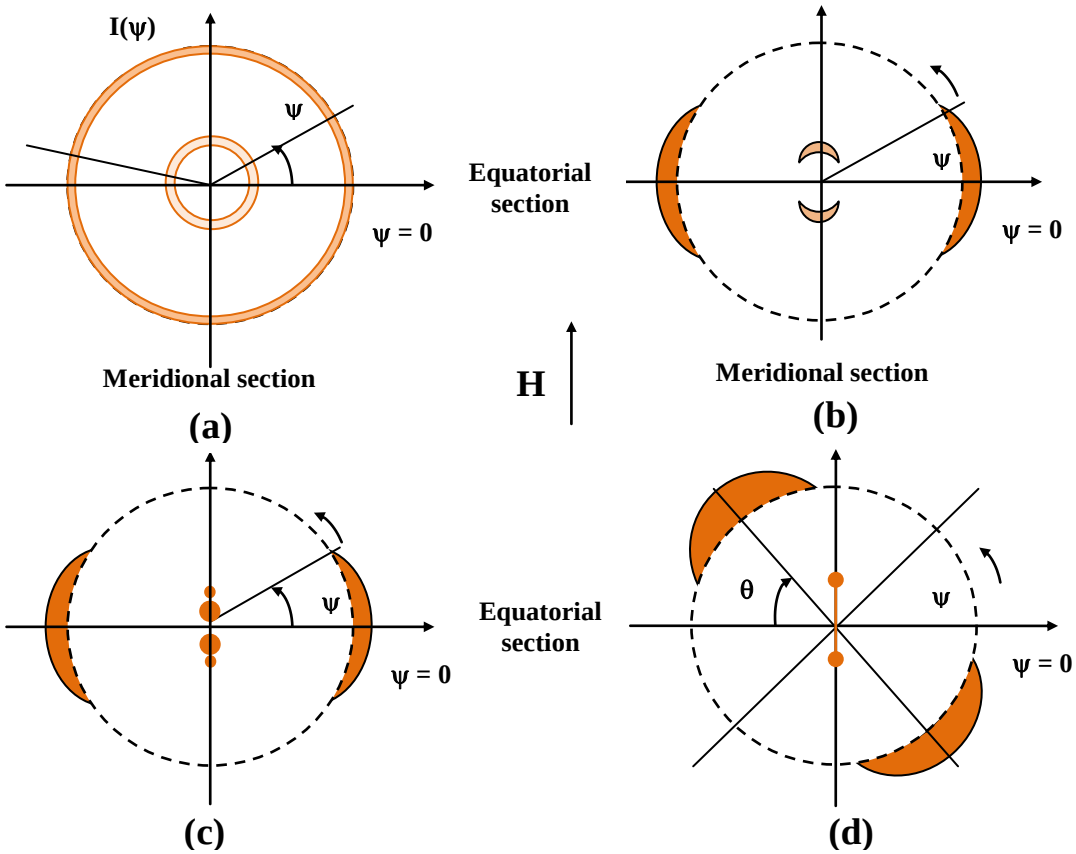

Figure 2.1(a-d) Schematic representation of x-ray diffraction pattern of (a) unoriented nematic, (b) nematic (c) smectic A (d) smectic C oriented perpendicular to the direction of the incident x-ray beam. θ and H is the tilt angle and applied magnetic field respectively.

The small angle x-ray diffraction pattern from a nematic liquid crystal oriented perpendicular to the direction of the incident x-ray beam is shown in the Figure 2.1(b).The main halo splits into two crescents for each of which intensity is maximum in the equatorial direction, *i.e.* perpendicular to the director. These crescents are formed mainly due to the intermolecular scattering and the corresponding Bragg angle is a measure of the lateral intermolecular distance. The angular distribution of the x-ray intensity I(ψ) vs. ψ curve, gives the orientational order parameter. In the meridional direction two crescents are also observed at much smaller angle and the corresponding Bragg angle is a measure of the apparent molecular length. The x-ray diffraction pattern of the smectic A phase is shown in Figure 2.1(c). The meridional spots are formed due to Bragg reflection from the layers and provide the value of the layer thickness. Since smectic A phase can have only quasi-long range order along its layer normal, second order Bragg reflections in the meridional direction are generally very weak and are often absent in the x-ray diffraction photographs.

The smectic C phase exhibit a tilted layered structure in which the smectic layer normal and the director are no longer collinear. Since there is no azimuthal preference for the tilt, the tilt occurs in different azimuthal direction as shown in Figure 2.1(d). For the smectic B phase, which is a three-dimensional ordered system with hexagonal symmetry, the outer diffraction ring is split up into six spots of strong intensity. Hence, the bond orientational order can be determined from the angular distribution of the x-ray intensity.

2.2.3.1 Linear scanning of x-ray photographs

The x-ray diffraction photographs, scanned by a high resolution scanner (HP Scanjet 5590) in the gray scale mode at 1200 dpi resolution have been analyzed using Origin software. The optical densities of the pixels were calculated and then converted to x-ray intensities with the help of a calibration curve following the procedure of Klug and Alexander [25].

2.2.3.2 Intermolecular distance

The average lateral distance [18] between the neighbouring molecules (D) is related to the corresponding Bragg angle ($2\theta_d$) according to the formula;

$$2D\sin\theta_d = k\lambda \tag{2.1}$$

where, $2\theta_d$ is the Bragg angle for the equatorial diffraction, λ is the wave length of the incident x-ray beam and k is a constant which comes from the cylindrical symmetry of the system. For perfectly ordered state, k = 1.117 as given by de Vries [26]. However, since the variation of the value of k on order parameter is known to be small, the value of k = 1.117 has been retained for all the calculation [26,27].

The longitudinal as well as the transverse in-plane correlation length in different mesophases have been determined from a linear scan of the inner and outer diffraction peaks. The intensity profile I(q) was then fitted to a Lorentzian form with a quadratic background [18],

$$I(q) = \frac{a_1}{a_2 + (q - q_0)^2} + a_3 q^2 + a_4 q + a_5 \tag{2.2}$$

Where, q is the magnitude of the scattering vector. Here a_1, a_2, q_0, a_3, a_4 and a_5 are the fitting parameters, which were adjusted to obtain the best fit. The position q_0 of the peak in the intensity profile has been used to determine the apparent molecular length. The correlation length is defined by

$$\xi = 2\pi(a_2)^{-1/2} \tag{2.3}$$

The equatorial intensity profile at wide angle have been fitted to estimate the transverse correlation length($\xi_{\parallel}$) while the longitudinal correlation length($\xi_{\perp}$) have been measured from the meridonial spread of the intensity profile at small angle arising from smectic-like fluctuations [18].

2.2.3.3 Apparent molecular length or layer thickness

To calculate the apparent molecular length (l) or the layer thickness (d), the Bragg equation (Equation 2.1) have been used, where θ_d is the Bragg angle for the meridional diffraction crescent or spot [19].

2.2.3.4 Tilt angle

The tilt angle (θ) has also been determined from the temperature variation of the layer thickness in SmA and SmC phase using the following equation [28-30]

$$\theta(T) = \cos^{-1}(d / d_A) \tag{2.4}$$

where, d is the layer spacing values in the SmC phase and d_A is the value of d in the SmA phase, measured at the SmA–SmC phase boundary.

2.2.4 Optical birefringence measurement

The nematic phase is optically uniaxial, strongly birefringent and possesses two refractive indices, which are important from application point of view. The principal refractive index of a nematic liquid crystal along and perpendicular to the molecular long axis are defined as extraordinary refractive index (n_e) and ordinary refractive index (n_o) respectively. The difference between the extraordinary and ordinary component of the refractive index is known as the optical birefringence (Δn), expressed as:

$$\Delta n = n_e - n_o \tag{2.5}$$

Optical birefringence (Δn) measurement [31-33] has been done by different methods. In the first method, the extraordinary and ordinary refractive indices (n_e, n_o) were determined by thin prism technique [34,35] and hence the birefringence ($\Delta n = n_e - n_o$) was evaluated. Secondly, a high resolution temperature scanning technique has been applied to determine the birefringence (Δn) of the samples in the different phases [36-40]. The well known Abbe refractometer has also been used to determine the refractive indices of few multi-component mixtures.

2.2.4.1 Thin prism technique

The principal refractive indices (n_e, n_o) of a liquid crystal sample have been measured by thin prism technique at a wavelength λ=632.8nm. Figure 2.2 illustrates the experimental setup for refractive index measurements. Thin prisms with refracting angle less than 2^o were prepared by using optically flat glass slides. First these slides were cleaned with detergent and water, and then treated in an acid mixture at a temperature of 60^oC for one hour. After that, the slides were washed with distilled water and further treated in 1 molar solution of KOH at 60^oC for the next one hour. Again the glass slides were washed with distilled water for several times. Finally, the glass plates were dipped into acetone to remove any organic impurities. A thin glass spacer was introduced between one of the vertical edge of the two glass slides to obtain the desired refracting angle of the prism. The glass plates of the prism were sealed together by using high temperature adhesive and were baked in an oven for few hours.

Liquid crystal (LC) samples were introduced into the prisms from its top open side by melting. The sample filled prism was alternately heated to isotropic phase and cooled slowly so that the liquid crystals were perfectly aligned with its optic axis parallel to the refraction edge of the prism. The prism was then placed inside a specially designed brass heater provided with a transparent opening at the centre and the temperature of the heater was maintained at the desired value by a Eurotherm temperature controller (PID 2404) within an accuracy of $\pm 0.1^oC$. The heater containing the LC filled prism was placed between the two pole pieces of an electromagnet by which a magnetic field (~ 1 Tesla) was applied to align the LC sample. A light beam (λ=632.8nm) from a He–Ne laser was allowed to be incident normally onto the prism. After passing through the aligned sample, the incident light beam splits into two components *i.e.* ordinary and extraordinary and two spots were visible on a screen. With the help of a high-resolution digital camera suitably interfaced with a computer, high-resolution digital images were obtained which were further processed to locate the center of the spots from where the ordinary (n_o) and extraordinary (n_e) refractive indices could be determined

within an accuracy of ±0.0006. The angle of the prism was first determined with the help of pure water.

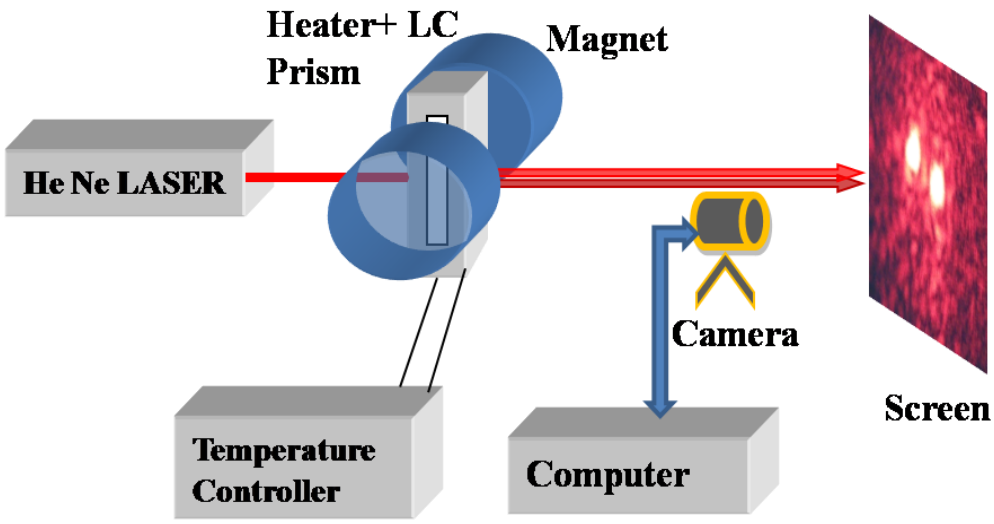

Figure 2.2 Schematic diagram of the experimental set-up for refractive index measurement using thin prism technique.

2.2.4.2 Optical transmission method

In the optical transmission (OT) method, the change in the transmitted intensity of a normally incident He-Ne laser beam (λ = 632.8nm) through a LC filled cell placed between a pair of crossed polarizers was recorded by a photo detector as a function of temperature [36-40]. The homogeneously aligned (planer geometry) (in a few cases homeotropically aligned) ITO coated cells were purchased from AWAT Co. Ltd., Warsaw, Poland. The temperature of the cell was controlled and measured with a temperature controller (Eurotherm PID 2404) with an accuracy of ±0.1°C by placing the cell in a brass heater. A precession multimeter (Keithley 2000) was used to measure the transmitted intensity of the laser beam. The optical birefringence (Δn) has been determined from the normalized transmitted intensity (I) data using the following equation [41-42]:

$$I = \frac{\sin^2 2\theta}{2}[1-\cos(\frac{2\pi\Delta nd}{\lambda})] \qquad (2.6)$$

where d is the LC cell thickness, θ is the angle made by the polarizer with respect to the optical axis and λ is the wavelength of the light used. In order to optimize the experimental measurements the angle between the polarizer and optical axis was fixed at 45^o.

The LC sample is believed to be a uniaxial birefringent medium with a spatially uniform orientation of the optic axis. The normalized transmitted intensity I(t) of the plane-polarized light passing through the LC sample of thickness d and birefringence Δn at normal incidence can be expressed as [41]:

$$I(t) = \left[\cos^2 \psi - \sin 2\phi \sin 2(\phi - \psi) \sin^2 \frac{\pi \Delta n d}{\lambda} \right] \tag{2.7}$$

where λ is the wavelength of the laser beam, ψ denotes the angle between polarizer and analyser and ϕ is the angle between the polarizer and the projection of the optic axis into the substrate plane. Equation 2.7 indicates that the resultant normalized transmitted light intensity ($I_1(t)$ - $I_4(t)$) can be obtained in four different orientations of the analyzer and polarizer:

(i) when $\phi = \theta$, $\psi = \pi/2$

$$I_1(t) = \sin^2 2\theta \sin^2 \frac{\pi d \Delta n}{\lambda} \tag{2.8}$$

Interestingly, Equation 2.8 is similar to Equation 2.6, used to determine the birefringence (Δn).

(ii) when $\phi = \pi/4 + \theta$, $\psi = \pi/2$

$$I_2(t) = \cos^2 2\theta \sin^2 \frac{\pi d \Delta n}{\lambda} \tag{2.9}$$

(iii) when $\phi = \theta$, $\psi = 0$

$$I_3(t) = 1 - \sin^2 2\theta \sin^2 \frac{\pi d \Delta n}{\lambda} \tag{2.10}$$

(iv) when $\phi = \pi/4 + \theta$, $\psi = 0$

$$I_4(t) = 1 - \cos^2 2\theta \sin^2 \frac{\pi d \Delta n}{\lambda} \tag{2.11}$$

From Equations 2.8-2.11 we can write

$$p_1 = \frac{I_1(t)}{I_1(t) + I_3(t)} = \sin^2 2\theta \sin^2 \frac{\pi d \Delta n}{\lambda} \tag{2.12}$$

$$p_2 = \frac{I_2(t)}{I_2(t) + I_4(t)} = \cos^2 2\theta \sin^2 \frac{\pi d \Delta n}{\lambda} \tag{2.13}$$

As the opposite tilt directions appear with the same light intensity, the parameters p_1 and p_2 remains invariant under a sign inversion of the tilt angle ($\pm\theta$). Therefore, Equation 2.12 and 2.13 are applicable for the SmC and SmC* phases. Using Equation 2.12 and 2.13 one can easily obtain the expressions for the tilt angle θ and birefringence Δn respectively,

$$\theta = \frac{1}{2} \tan^{-1} \left(\frac{p_1}{p_2}\right)^{\frac{1}{2}} \tag{2.14}$$

$$\Delta n = \frac{\lambda}{\pi d} \sin^{-1} (p_1 + p_2)^{\frac{1}{2}} \tag{2.15}$$

The values of the tilt angle (θ) determined from the optical transmission method are found to be about 10 percent lower than those determined from the x-ray diffraction technique. Due to the difficulty in achieving a perfectly uniform and defect-free alignment, a slight light leakage was observed even in the well aligned SmA phase with the average tilt angle (θ) parallel to one of the polarizers. This transmission value, which theoretically should be zero, was therefore subtracted from all the measured intensity values. This method is well suited for the tilt angles above 5^o but for $\theta=0^o$ the errors may have a larger effect.

2.2.4.3 Determination of orientational order parameter

A number of methods have been developed to determine the orientational order parameter (S) in the liquid crystalline phases. However, the optical method is the most commonly used owing to its simplicity as well as accuracy. The usual technique for the evaluation of the long range order parameter from optical

methods necessitates the measurement of both the ordinary and extraordinary refractive indices (n_o and n_e) as well as the density (ρ) data. In such cases, using these three measured quantities, either the standard Vuk's isotropic model [43] or the Neugebauer's relations based on the anisotropy of the internal field [44] are adopted to determine the principal polarizabilities parallel and perpendicular to the molecular long axes and hence, the anisotropy of the molecular polarizabilities ($\Delta\alpha$) can be calculated. The polarizability anisotropy ($\Delta\alpha_0$) in the perfectly ordered crystalline state is determined from the well-known Haller's extrapolation procedure [45] and the order parameter is calculated from the ratio $\Delta\alpha/\Delta\alpha_0$. According to de Jue [46], the variation of density (ρ) over the nematic phase is usually small and the temperature dependence of the optical birefringence (Δn) gives a good indication of the variation of orientational order parameter with temperature. Furthermore, Kuczynski *et al.* [47] have also shown that the order parameter determined directly from the birefringence measurements are consistent with the S values obtained from the polarizability data. Therefore, in this work, the order parameter (S) has been determined using only the refractive indices and the birefringence data.

The temperature dependence of optical birefringence (Δn) in the nematic phase can be described by a power law expression having the following form [45]:

$$\Delta n = \Delta n_0 \left(1 - \frac{T}{T^*}\right)^{\beta} \tag{2.16}$$

where Δn_0, T* and β are adjustable parameters. T* is about 1-3K higher than the clearing temperature and the exponent β depends on the molecular structure and its value is close to 0.2. Δn_0 is the birefringence in the completely ordered state *i.e.* at the absolute zero temperature. Moreover, the temperature dependent birefringence is related to the order parameter (S) by the following expression [46]:

$$S \approx \frac{\Delta n}{\Delta n_0} \tag{2.17}$$

This direct extrapolation method offers a very useful technique to determine the order parameter from the high resolution Δn data and excludes the requirement of individual refractive indices as well as density values.

2.2.5 Dielectric permittivity measurement

The static dielectric permittivity measurements provide important information about the dipole organization and dipole-dipole interaction in the mesophases. Planar and homeotropically aligned ITO coated liquid crystal cells with unidirectionally rubbed polyimide layers having thickness 8.9μm were procured from AWAT Co. Ltd., Warsaw, Poland and were used for filling the samples. The capacitance of the LC filled cells was measured at frequency of 1kHz, as a function of temperature, using a digital LCR-bridge (Agilent E4980A) with a relative accuracy of about 0.05% [48-53]. The temperature of the sample was controlled and measured with an accuracy of ±0.1^{o}C by placing the cell in a brass heater suitably connected with a temperature controller (Eurotherm PID 2404). For this study, the cell was first calibrated by measuring the capacitances of standard dielectric liquids within an accuracy of 1%. The parallel and perpendicular components of the dielectric permittivity ($\varepsilon_{\parallel}$ and $\varepsilon_{\perp}$) were determined by measuring the capacitances $C_{\mathbf{a}}$, $C_{\mathbf{b}}$ and $C_{\mathbf{x}}$ of the cell filled with air, benzene (as standard materials) and the liquid crystal sample respectively, by applying an electric field parallel and perpendicular to the director and using the following expression

$$\varepsilon_x = 1 + \frac{(C_x - C_a)}{(C_b - C_a)}(\varepsilon_b - 1) \tag{2.18}$$

where ε_b and ε_x are the relative permittivities of benzene and the liquid crystalline substance and that of the air is taken as unity.

The complex dielectric permittivities were also determined with the help of HP 4192A impedence analyzer covering the frequency (f) ranges 1kHz to 30MHz at the Institute of Physics, Jagiellonian University in Krakow. The LC samples were oriented in a magnetic field of strength ~ 0.7 Tesla in the nematic phase. The

real (ε') and imaginary (ε'') component of the complex dielectric permittivity can be determined from the following equations

$$\varepsilon' = C_x/C_a \tag{2.19}$$

$$\varepsilon'' = \sigma/(2\pi f C_a) \tag{2.20}$$

where σ is the conductivity of the sample filled LC cell.

2.2.6 Dipole moment measurement

The dipole moment (μ) has been measured by using the Guggenheim method [54] which is based on the Debye equation. The dielectric permittivity (ε) and refractive index (n) of the compound dissolved in a non-polar solvent *p*-xylene were measured as a function of molar concentration (c) at 30^{o}C to determine the dipole moment. The dielectric permittivities were determined by measuring the capacitance of a solution filled cell at 1 kHz by using Agilent E4980A digital LCR-bridge and the refractive index of the solution was measured by thin prism technique [34,35]. According to the Guggenheim [55,56], the effective dipole moment (μ) of a molecule in solution of molar concentration c at room temperature can be written as [54]:

$$\mu^2 = \frac{27k_\beta T[(\varepsilon_2 - n_2^2) - (\varepsilon_1 - n_1^2)]}{4\pi N(\varepsilon_1 + 2)(n_1^2 + 2)c} \tag{2.21}$$

where, the suffixes 1 and 2 respectively refer to the solvent and solution parameters, k_β is the Boltzmann constant, T is the absolute temperature and N is the Avogadro number. The dipole moment determined at different concentrations has been plotted as a function of weight percentage of the solute and an extrapolation of the fitted curve to infinite dilution gives the value of the same for an isolated molecule. The experimental value of the dipole moment (μ) has been compared with those obtained from the semi-empirical molecular orbital package MOPAC [57,58] for all the compounds investigated, in their minimum energy configuration.

2.2.7 Splay elastic constant measurement

In the nematic phase, the liquid crystal director may vary spatially due to the application of an external field. The deformations of a nematic phase can be traced back to three fundamental elastic deformations: splay, bend and twist (Figure 2.3(a-c)). In the deformed state, there exists an elastic restoring force which tries to bring the system into the equilibrium configuration. Generally, each of the deformation modes is characterized by an individual elastic constant. These elastic constants of the liquid crystals can be determined by different techniques. One of the simplest and most convenient method to obtain the elastic constant is the electric field induced Freedericksz transition [9,10] as shown in Figure 2.4(a-b).

For the splay elastic constant (K_{11}) measurement, the LC sample was cooled from the isotropic phase to the nematic phase and a sinusoidal voltage of frequency 1kHz was applied [59-62] after the sample stabilized at a particular temperature. The applied voltage was increased in small steps from a value lower than the Freedricksz threshold [9,10] voltage to 20V rms. Agilent E4980A precession LCR-bridge was used to record the cell capacitance as a function of the applied voltage. The capacitance value changes rapidly near a certain voltage which is called the threshold voltage (V_{th}) for Freedericksz transition (Figure 2.5). Using the value of the threshold voltage (within ±0.5%) the splay elastic constant (K_{11}) was calculated from the well known equation

$$K_{11} = \frac{\varepsilon_0 \Delta\varepsilon V_{th}^2}{\pi^2} \tag{2.22}$$

where ε_0 is the free space permittivity.

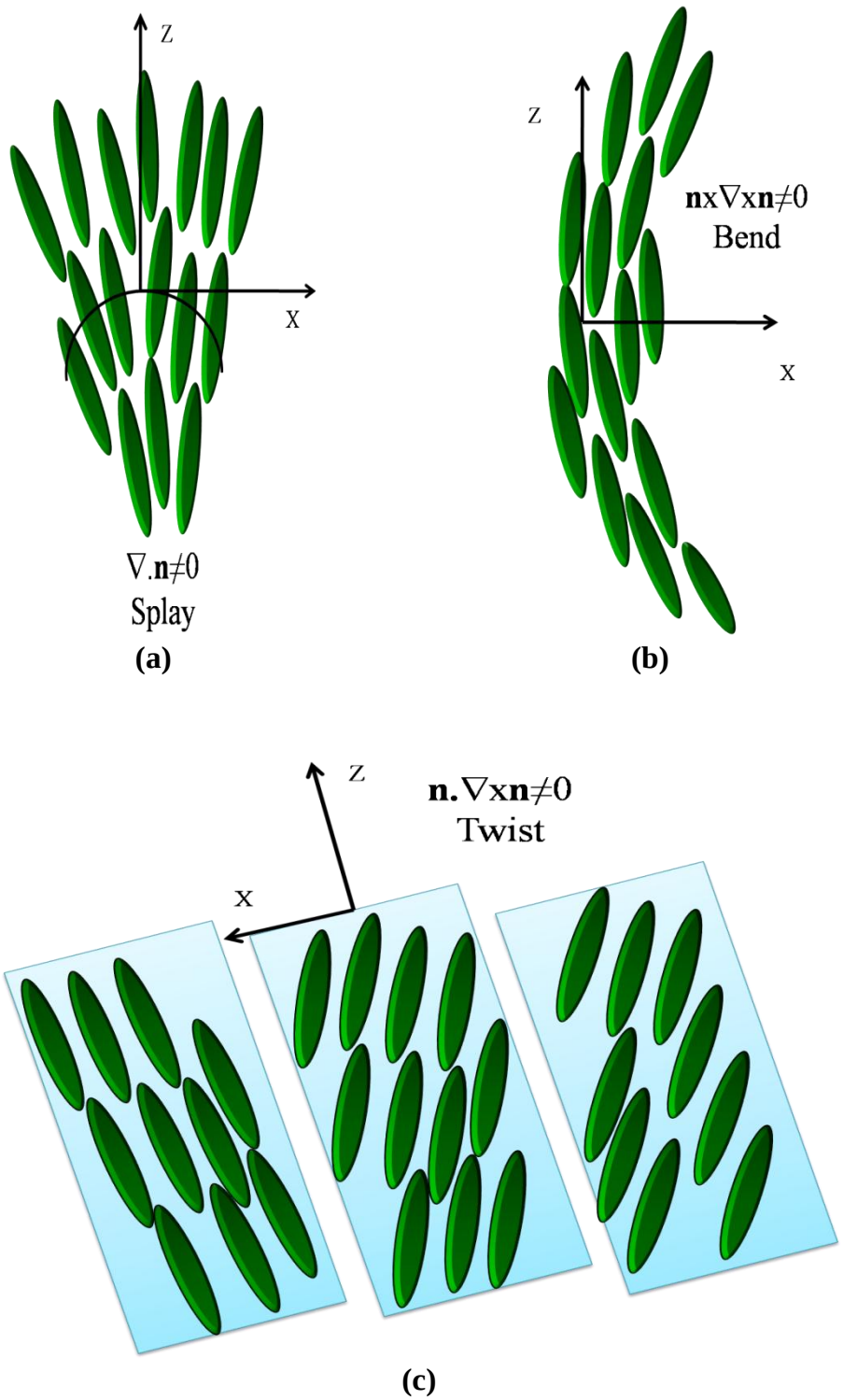

Figure 2.3(a-c) Schematic diagram of an ordered nematic liquid crystal in three different deformation states: (a) splay, (b) bend and (c) twist.

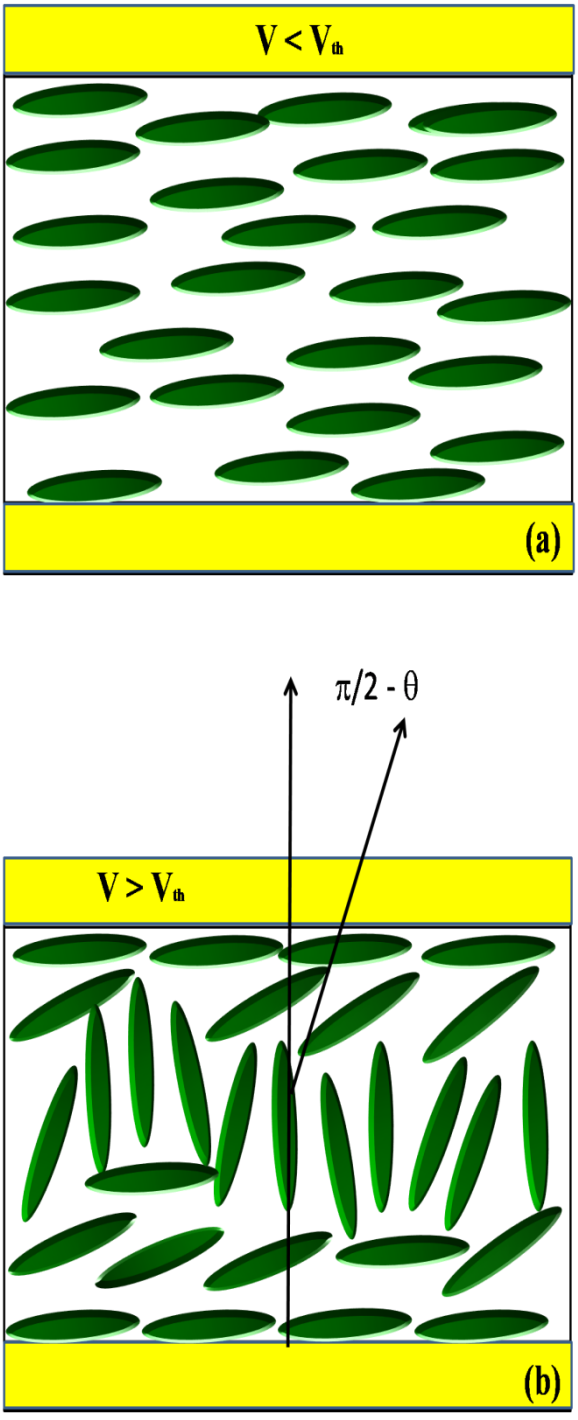

Figure 2.4(a-b) Schematic representation of director configuration: (a) below threshold field (V_{th}) (b) above the threshold field (V_{th}).

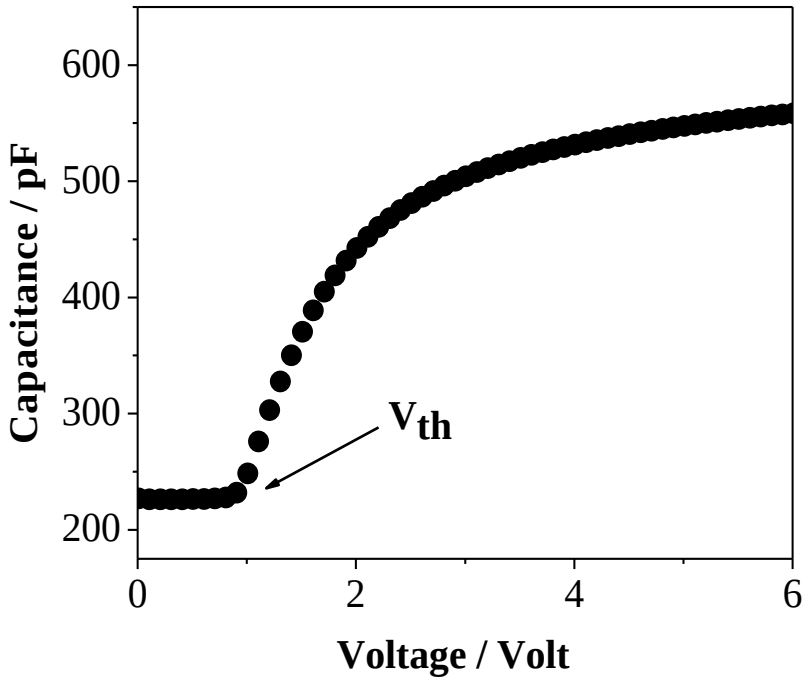

Figure 2.5 Voltage dependent capacitance change due to Freedricksz transition in a liquid crystal.

2.2.8 Rotational viscosity measurement

Rotational viscosity (γ_1) of liquid crystals represents an internal friction between the directors during a rotation process. The magnitude of the rotational viscosity depends on the intermolecular structure, molecular association and also on the temperature. A relaxation technique [63-65] was used to probe the rotational viscosity (γ_1). In this method, a He-Ne laser beam (λ = 632.8nm) was allowed to pass through a homogeneously aligned ITO coated LC cell (procured from AWAT Co, Warsaw, Poland) of thickness 8.9μm placed between two crossed polarizers oriented at 45^o to the director. The temperature of the cell was regulated and measured by a temperature controller (Eurotherm PID 2404) with an accuracy of ±0.1^{o}C by placing the cell in a brass heater with glass windows [61,65]. The schematic representation of the experimental set up for measuring the rotational viscosity is shown in Figure 2.6.

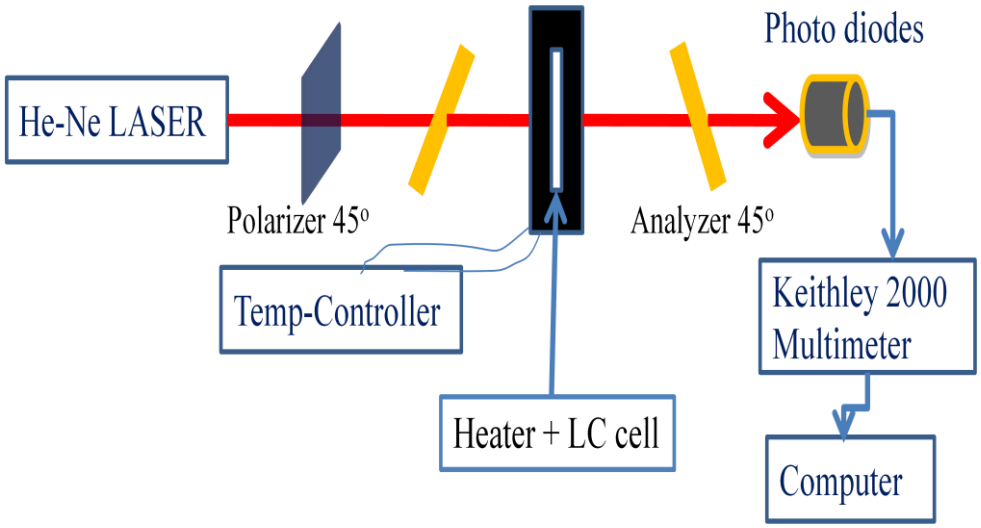

Figure 2.6 Experimental set up for determining rotational viscosity.

When a linearly polarized light impinges in a parallel-aligned cell, if the polarization axis is parallel (*i.e.* the angle between the polarizer and the optic axis, $\theta = 0^{o}$) to the LC director, a pure phase modulation is achieved because light now behaves as an extraordinary ray. On the other hand, if the angle $\theta = 45^{o}$, then phase retardation occurs due to the different propagating speed of the extraordinary and ordinary rays in the liquid crystalline medium. The resultant phase retardation (δ) is determined by the LC layer thickness d and the effective birefringence, $\Delta n(V, T, \lambda)$, which is dependent on the applied voltage, temperature and wavelength λ of the incident light and can be written as [66,67]

$$\delta (V,T,\lambda) = 2\pi d\Delta n (V,T,\lambda) \qquad (2.23)$$

At V = 0, Δn ($= n_e - n_o$) has its maximum value. However, in the $V > V_{th}$ regime, the effective birefringence decreases sharply as voltage increases, and then gradually saturates. The slope depends on the elastic constants, dielectric permittivity and refractive indices of the LC material. At $V >> V_{th}$ regime, basically all the bulk directors are aligned by the field to be perpendicular to the

substrates, except the boundary layers. Thus, further increase in voltage only causes a small change in the orientation of boundary layers. In this regime, the effective birefringence is inversely proportional to the applied voltage. The advantage of operating an LC device at low voltage regime is that a large phase change can be obtained merely with a small voltage swing. However, the value of the relaxation time is relatively higher [63].

The transmitted light intensity was measured as a function of applied voltage by using a photodiode which was connected to a digital storage oscilloscope (Agilent 54622A DSO). Figure 2.7 depicts the voltage dependent transmittance curve. A voltage (V_B) corresponding to the first maximum or minimum in the transmitted intensity was applied to the LC cell. When the voltage V_B was removed at t = 0, the optical transmission decreases and the phase change $\delta(t)$ could be calculated from the time dependent intensity, I(t), according to the following equation [61,65]:

$$I_t = I_o \sin^2\{(\frac{2\pi d\Delta n}{\lambda} - \delta(t))/2\} \qquad (2.24)$$

where I_o is the maximum intensity change. Therefore, the relaxation time [61,65] was determined from the equation given by [63]

$$\delta(t) = \delta_0 \exp(-\frac{2t}{\tau_0}) \qquad (2.25)$$

where δ_0 is the total phase change of the sample under the applied bias voltage V_B. A plot of $\ln(\delta(t)/\delta_0)$ with time (t), yields a straight line with slope $(2/\tau_0)$ and from the slope, the value of decay time τ_0 can be determined.

Moreover, $\delta(t)$ becomes $\delta_0\exp(-4t/\tau_0)$ in Equation 2.25 when the value of δ_0 is around $N\pi$ (N= integer). Again applying the voltage V_B to the liquid crystal cell the rise time τ_{rise} was obtained in the similar way. The accuracy of the relaxation time measurement was found to be ±5ms. Thus, by measuring the relaxation time

τ_0 and from the knowledge of the splay elastic constant K_{11} and the cell gap d, the rotational viscosity γ_1 was determined from the following equation [61,63,65,68]:

$$\gamma_1 = \frac{\tau_0 K_{11} \pi^2}{d^2} \tag{2.26}$$

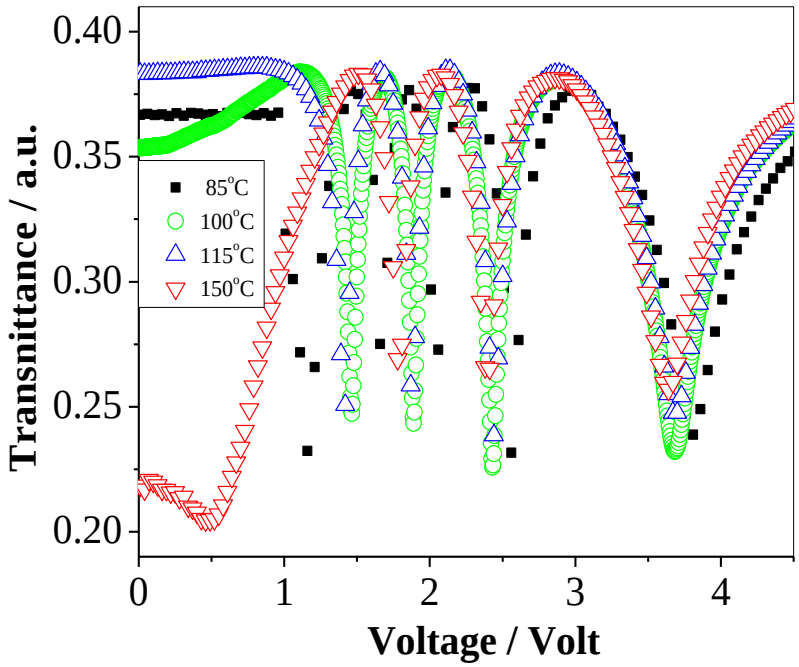

Figure 2.7 Voltage dependent optical transmittance of a liquid crystal placed inside 8.9μm thick planar liquid crystal cell at different temperatures.

2.2.9 Activation energy

The temperature dependence of the rotational viscosity (γ_1) was fitted to the following expression [61]

$$\gamma_1 = \gamma_0 S \exp\left(\frac{E_a}{k_\beta T}\right) \tag{2.27}$$

where k_β is the Boltzmann constant and E_a is the associated activation energy. S is the orientational order parameter which was determined from the birefringence

measurement and γ_0 is the fitting parameter. From the slope of the ln(γ_1/S) vs 1/T curve the activation energy E_a can be evaluated.

2.2.10 Figure of merit

The response time (τ_0) is proportional to d^2. Therefore comparative study of τ_0 is not possible unless the cell gap exactly matches its birefringence in order to determine the best possible response times. Figure of merit (FoM) completely eliminates the necessity of matching the cell gap and helps to compare the potential applicability of a particular compound in a display device. FoM is defined as [69,70]:

$$FoM = \frac{K_{11}\Delta n^2}{\gamma_1} \tag{2.28}$$

where K_{11} is the splay elastic constant, Δn is the birefringence and γ_1 is the rotational viscosity. All of these parameters are temperature dependent. Furthermore, both the birefringence and elastic constant [46,69,71,72] are dependent on the order parameter S and can be approximated as:

$$\Delta n = (\Delta n_0).S \tag{2.29}$$

$$K_{11} = A_0.S^2 \tag{2.30}$$

The temperature dependent FoM is derived as:[69]

$$FoM = \left(\frac{A_0}{b}\right)(\Delta n_0)^2\left(1-\frac{T}{T_C}\right)^{\beta}\exp\left(-E_a / k_\beta T\right) \tag{2.31}$$

where Δn_0 is the birefringence when S =1 *i.e.* in the perfectly ordered state, E_a is the activation energy of the liquid crystal and k_β is the Boltzmann constant. The value of the parameter β is around 0.20 and depends on the molecular structures. The FoM strongly depends on the temperature [69]. It first increases with increasing temperature and reaches a maximum value at certain temperature called the operating temperature. As the temperature approaches the clearing temperature T_C, the birefringence has very steep drop which causes a sharp decrease in the Figure of Merit. The higher Figure of Merit a LC possesses, the faster response

time it exhibits. Thus operating a LC device at an elevated temperature is beneficial for reducing response time. However, it brings complication to the driving scheme since this necessitates additional temperature control system.

2.2.11 Electro-optic measurement

For the electro-optic studies, 5μm thick ITO coated planar glass cells (procured from AWAT Co. Ltd., Warsaw, Poland) have been used. The inner surfaces of the glass plates were polymer buffed to align the sample in the planar configuration. The liquid crystalline (LC) sample was introduced into the cell by capillary action at high temperature in the isotropic state. Eurotherm PID 2404 temperature controller was used to control the temperature of the LC filled cell, placed within a specially constructed heater with an accuracy of ±0.1ºC. The alignment of the sample was achieved by slowly cooling of the sample from the isotropic to the smectic phase by applying a high square wave electric field (10 V/μm) at a low frequency (50 Hz). After the alignment of the LC cell in the bookshelf geometry, the applying voltage was removed and the sample were further cooled to the SmC* or SmC_A* phase. It was assumed that compounds having longer pitch retained their surface alignment in the 5μm thick cells upon transition to the SmC* and SmC_A* phases. The spontaneous polarization of the ferro and antiferroelectric LC was determined using the polarization reversal technique [73-75].

A square wave electric field V (40 Vpp) at 50 Hz was applied to the LC sample. The input voltage was applied by the Picotest (G5100A) arbitrary waveform generator and the FLC (F20A) voltage amplifier. As the polarization was inverted by the applied field, a current pulse was observed. The re-polarization current response was fed to the Agilent Digital Storage Oscilloscope 1052B suitably interfaced with a computer through a resistance (22KΩ), connected to the LC cell in series. Figure 2.8 illustrates the block diagram of the circuit used for the measurement of spontaneous polarization.

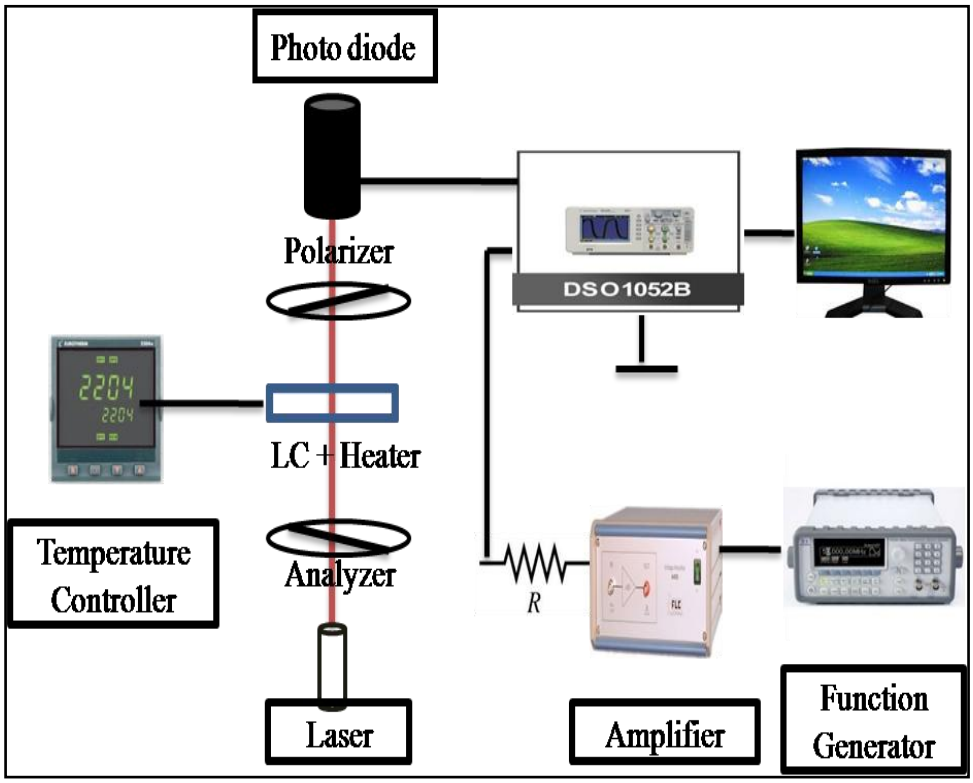

Figure 2.8 Experimental set up for electro-optic study using polarization reversal technique.

The liquid crystal may be regarded as a resistance (R) connected to a capacitor (C) in parallel. Therefore, the output current is the sum of three currents: (i) I_C, due to charge accumulation in the capacitor (ii) I_P, due to polarization realignment and (iii) I_I for the ionic current [73]. The total output current can be written as

$$I = I_C + I_P + I_I = C\frac{dV}{dt} + \frac{dP}{dt} + \frac{V}{R} \tag{2.32}$$

where P is the amount of charge induced when the spontaneous polarization (P_s) changes sign after reversal of the electric field. The contribution from I_C and I_I can be removed by choosing an appropriate baseline of the output current response curve (a hump) using mathematical software. Hence the magnitude of the

spontaneous polarization was determined from the area (A) under the current reversal peak using the following formula [74]

$$P_S = \frac{1}{2A}\int Idt \qquad (2.33)$$

To estimate the precision of the experimental setup, the spontaneous polarization of pure (S)MHPOBC (4-(1-methylheptyloxy)carbonylphenyl4'-octyloxy-4-biphenyl carboxylate), procured from Sigma Aldrich, [73-78] have also been determined by applying voltage of square waveform. The experimentally obtained P_S values [74] agree quite well with those obtained by others [77,78] as shown in Figure 2.9. In this study, the values of the spontaneous polarization have been measured with a precision of ±0.9 nC/cm^2.

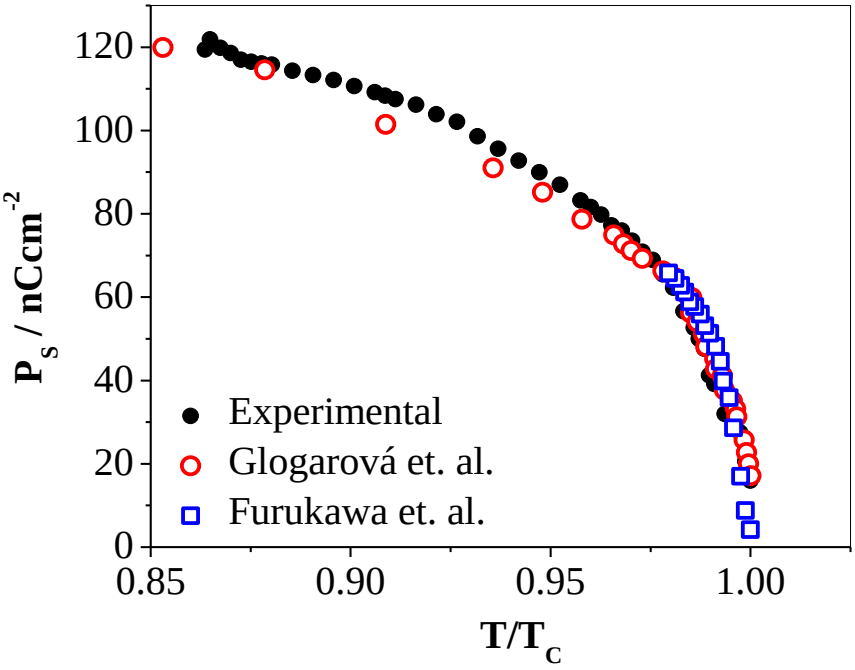

Figure 2.9 Temperature dependent spontaneous polarization (P_S) curve of (S)MHPOBC.

The free relaxation time τ for the ferroelectric or antiferroelectric liquid crystal director were also evaluated from the time ($\tau_{10\text{-}90}$) required to change the current from 10% to 90% of the peak value of the hump of the re-polarization

curve upon switching [79]. The relation between the relaxation time and $\tau_{10\text{-}90}$ is given by [74,79]:

$$\tau = \frac{t_{10-90}}{1.8} \tag{2.34}$$

Hence, the effective torsional bulk viscosity (η) has been determined by using the following relation:

$$\eta = P_S E \tau \tag{2.35}$$

where E is the applied switching electric field. The free relaxation time (τ) and the effective torsional bulk viscosity were determined with a precision of ±1μs and ±0.9 Pa.s respectively. Moreover, the anchoring energy (F) of the ferroelectric liquid crystal (FLC) system is given by [79-81]

$$F = \int_S \left(\tilde{W}_D + \tilde{W}_P\right) d\sigma \tag{2.36}$$

where $\tilde{W}_D = W_D (P_S n)^2$ and $\tilde{W}_P = W_P (P_S n)$

W_D and W_P are the dispersion and polarization anchoring strength coefficients respectively, and **n** is the layer normal. Measuring the free relaxation time τ and the spontaneous polarization (P_S) one can determine the dispersion anchoring strength coefficient, W_D using the following equation [79-84]:

$$W_D = \frac{\eta d}{4\tau} \tag{2.37}$$

For sufficiently large values of the cell thickness d, the effect of surface anchoring is negligibly small and the helical states become more favorable. The existence of a threshold field (E_{th}) above which the bi-stable state appears is given by [79,81]:

$$E_{th} = \frac{\sqrt{W_D}}{K} \tag{2.38}$$

where K is the average elastic constant and W_P is assumed to be zero. With increasing anchoring, the switching amplitude of the electric field has to be increased. For $W_D = 0$, the bi-stability threshold (E_{th}) follows the relation [79,81]

$$E_{th} = \frac{W_P^2}{KP_S} \tag{2.39}$$

The polar interaction of the FLC director with a substrate is directly proportional to the spontaneous polarization. Combining Equation 2.38 and 2.39 the polarizing anchoring strength coefficient W_P can be written as [79-84]:

$$W_P = \sqrt{P_S \sqrt{W_D}} \tag{2.40}$$

The advantage of the proposed method is that the different characteristic parameters (P_s, τ, η, W_D and W_P) can be determined in a single experiment, from the relaxation voltage curves corresponding to the re-polarization current of a liquid crystal cell. Moreover, to study the V shaped switching a solid state laser beam (λ = 532nm) was allowed to pass through the LC cell, placed between two crossed polarizer oriented at 45º to the director. The transmitted light intensity was recorded as a function of the applied electric field using a photodiode in conjunction with Agilent Digital Storage Oscilloscope, 1052B, suitably interfaced with the computer.

2.3 Theoretical background

2.3.1 Maier-Saupe theory for the nematic phase

A number of theories have been developed in order to explain the behaviour of the nematic phase but the most successful theories are those which are based on the molecular mean field approximation. Maier and Saupe [1-3] have given a molecular statistical theory of the nematic phase (N) and nematic to isotropic (N-I) phase transition based on the molecular mean field approximation.

In this case, the constituent molecules of the nematic phase have been assumed to be rod-like and under the influence of an average field owing to all the other molecules of the LC system. This rod-like molecules possesses cylindrical symmetry and tends to orient their molecular long axis along a preferred direction (**n**), called the director. Maier and Saupe [1-3] assumed that the nematic ordering is caused by the anisotropic part of the dispersion interaction between the molecules and also considered the following points:

i) As far as the long range nematic ordering is concerned the influence of the permanent dipoles can be neglected.

ii) The effect of induced dipole-dipole interaction plays an important role and need to be considered.

iii) The distribution of the centre of mass of the neighbouring molecules is considered to be spherically symmetric.

iv) The molecules possess cylindrical symmetry with respect to the molecular long axis.

In the nematic phase, the molecular long axis makes an angle (θ) with the director, hence the distribution of molecular long axis about the director can be represented by an orientational distribution function f(cosθ). Moreover, different experimental results reveal that the rod-like nematic molecules possesses up-down symmetry *i.e.* the heads and tails of the molecules are not distinguishable separately. This makes the orientational distribution function f(cosθ) an even function of cosθ. Thus f(cosθ) can be written as,

$$f(\cos\theta) = \sum_{L-even} \frac{(2L+1)}{2} < P_L(\cos\theta) > P_L(\cos\theta) \qquad (2.41)$$

where $P_L(\cos\theta)$ are the L^{th} even order Legendre polynomials and $<P_L(\cos\theta)>$ is the statistical average given by

$$< P_L(\cos\theta) >= \int_0^1 P_L(\cos\theta) f(\cos\theta) d(\cos\theta) \qquad (2.42)$$

$<P_L>$ are known as the orientational order parameters and the first term *i.e.* $<P_2>$ is generally called order parameter. It is also sometimes denoted by S. In the

isotropic phase (high temperature phase) $<P_2>$ = 0 and in perfectly ordered state *i.e.* crystalline state $<P_2>$ =1. Humphries *et al.* [85] has given a more comprehensive idea considering the deviations from the spherical symmetry of the pair potential correlation function of the molecules. From the mean field theory the single molecule potential function V(cosθ) of the cylindrically symmetric molecules can be written as

$$V(\cos\theta) = \sum_{L-even} U_L < P_L > P_L(\cos\theta) \quad (L\neq 0) \tag{2.43}$$

where U_L are the functions of distance between the central molecule and its neighbours only. Putting L = 2 in Equation 2.42 we get

$$< P_2(\cos\theta) >= \int_0^1 P_2(\cos\theta)\, f(\cos\theta) d(\cos\theta) \tag{2.44}$$

Keeping the first term (L=2) of the right hand side of Equation 2.43, the expression for the potential energy function of a single molecule can be written as

$$V(\cos\theta) = -vP_2(\cos\theta) < P_2 > \tag{2.45}$$

where $v = -U_2$. Therefore, the orientational distribution function for a single molecule is given by

$$f(\cos\theta) = Z^{-1} \exp[-V(\cos\theta)/k_\beta T] \tag{2.46}$$

where k_β is the Boltzmann's constant and Z is the single molecule partition function given by

$$Z = \int_0^1 \exp[-V(\cos\theta)/k_\beta T] d(\cos\theta) \tag{2.47}$$

Substituting the value of f(cosθ) and Z from Equations 2.46 and 2.47 into Equation 2.44 one can write

$$< P_2(\cos\theta) >= \frac{\int_0^1 P_2(\cos\theta) \exp[P_2(\cos\theta) < P_2 > /T^*] d(\cos\theta)}{\int_0^1 \exp[P_2(\cos\theta) < P_2 > /T^*] d(\cos\theta)} \tag{2.48}$$

where $T^* = k_\beta T / v$

Equation 2.48 is a self-consistent equation as it contains $<P_2>$ on both sides and can be solved by iterative method to obtain the temperature dependence of $<P_2>$. For every temperature (or T*) there is $<P_2>$ value which satisfies the self-consistent equation. Now, for all temperatures $<P_2> = 0$ is a solution which corresponds to the isotropic phase while for temperatures $T^* < 0.22284$, two other solutions to Equation 2.48 appear. It has been observed that the nematic phase ($<P_2> > 0$) is the stable one when the temperature T* satisfies the condition $0 \leq T^* \leq 0.22019$ while for $T^* > 0.22019$, a thermodynamically stable isotropic phase with $<P_2> = 0$ is obtained. With the increase in temperature, the order parameter $<P_2>$ shows a decreasing trend from unity to a minimum value of 0.4289 at T*=0.22019. At T*=0.22019 the N-I phase transition takes place with a discontinuous change in the order parameter $<P_2>$ from 0.4289 to 0 indicating a first order nature of the phase transition. The entropy change near the phase transition is a measure of the order of the transition. For the N-I phase transition the change in the entropy is near about 0.830 cal/moleK, which is comparatively much smaller than that of the solid to liquid transition in which entropy change is approximately 25 cal/mole-K. So these phase transitions are often called weakly first order phase transition. Temperature dependent $<P_2>$ values can be calculated by solving the Equation 2.48 iteratively. In spite of the approximations that are entailed in the Maier-Saupe mean field theory, for a number of nematic LC, the experimentally determined $<P_2>$ values agrees quite well with those predicted by the theoretical Maier – Saupe values [86-88] .

2.3.2 Elastic continuum theory

Although the molecular theories of liquid crystals can successfully explain a number of physical properties of the mesophases but there exists a class of phenomena which involves bulk liquid crystal samples with respect to which the molecular theory is not so useful. Therefore, in describing these bulk properties or its response to external perturbations, the liquid crystal system has to be considered as a continuous media [5] with a set of elastic constants. Oseen [6**]**,

Zocher [7] and Frank [8] developed a static continuum theory for uniaxial liquid crystals that has proved to be very much effective in describing the field (electric or magnetic) induced effects. In the nematic phase, the uniform parallel orientation of the directors corresponds to a state of minimum free energy *i.e.* an equilibrium state. By applying some external force such as electric field or magnetic field, the orientation of the director can be changed. In this way the nematic liquid crystals is deformed, thereby increasing the free energy of the system. The deformed state thus formed corresponds to a state with higher free energy than the equilibrium state. In general, there are three fundamental types of elastic deformations in case of nematics to which all the deformations can be characterized: the splay, bend and twist deformations.

According to the continuum theory of liquid crystals, the free energy per unit volume of a deformed liquid crystal relative to its equilibrium state can be written in terms of three independent elastic constants which are related to the splay, twist and bend deformations:

$$F_{def} = \frac{1}{2}[K_{11}(\nabla \cdot n)^2 + K_{22}(n \cdot \nabla \times n)^2 + K_{33}(n \times \nabla \times n)^2] \qquad (2.49)$$

where, K_{11}, K_{22}, K_{33} are known as the splay, twist and bend elastic constants respectively, collectively known as the Frank elastic constants and **n** is the director. The elastic constants should have the dimension energy/length. It is very much possible to produce purely splay, twist or bend deformations; therefore all the elastic constants (K_{11}, K_{22}, K_{33}) are positive quantity [89] and also the free energy F_{def} must be positive in order to give stability for the uniformly aligned state.

2.3.3 Freedericksz transition

Electric field has a strong effect on the liquid crystalline materials. When a planar ITO coated cell is filled with liquid crystal, there is a strong influence of planar anchoring, *i.e.* the director is essentially locked in an orientation parallel to the sample plane at the bounding surfaces. Because of the elastic properties of the nematic phase this surface imposed alignment is propagated through the liquid

crystal in order to minimize the deformations in director which would increase the energy. When an electric field is applied there is a competition between the dielectric contribution to the free energy, promoting a reorientation of the director, and the elastic contribution, counteracting any change from the initial planar-aligned state. At weak fields the elastic contribution wins and the director remains unaffected by the field whereas at strong fields it is the other way around and the sample is switched. The borderline case is called the Freederiksz threshold. The switching process is called the Freederiksz transition [9,10].

To solve the steady state directors' distribution, the total free energy of the system needs to be minimized. The total free energy for the nematic phase consists of two parts: (1) dielectric free energy which originates from the interaction between the applied field and anisotropic LC molecules and (2) elastic free energy which originates from the elastic deformation. On the other hand, to derive the dynamic response of the LC directors, the elastic torque and the electric field-induced torque need to balance with the viscous torque.

In a parallel aligned nematic LC cell, the directors are along the *x* axis and the two bounding surfaces are at Z=0 and Z = d. When the applied voltage V (along the z axis) exceeds the Freedericksz threshold V_{th}, the LC undergoes an elastic deformation. The directors then tilt in the *xz* plane, the amount of tilt $\phi(z)$ being a function of the distance from the aligning surface. $\phi(z)$ has a maximum value ϕ_m at $Z = d/2$ and $\phi(z) = 0$ at the boundaries. In case of a static deformation of LC directors, the Oseen-Frank equation describes the balance between an elastic torque and electric torque exerted by the applied field and can be written as [46]

$$(K_{11}\cos^2\phi + K_{33}\sin^2\phi)\left(\frac{d^2\phi}{dz^2}\right) + (K_{33} - K_{11})\sin\phi.\cos\phi\left(\frac{d\phi}{dz}\right)^2 = \varepsilon_0\Delta\varepsilon E^2\sin\phi.\cos\phi \quad (2.50)$$

where, K_{11}, K_{22}, and K_{33} stand for splay, twist and bend elastic constants respectively, and V_{th} is the Freedericksz threshold voltage given by

$$V_{th} = \pi\sqrt{\frac{K_{11}}{\varepsilon_0\Delta\varepsilon}} \quad (2.51)$$

However, in the dynamic response, the viscous torque which opposes the directors' rotation has to be included. The most general treatment of the dynamic of LC directors is described by the Erickson-Leslie equation [90-93]:

$$\frac{\partial}{\partial z}[(K_{11}\cos^2\phi + K_{33}\sin^2\phi)\frac{\partial\phi}{\partial z}] + (K_{33}-K_{11})\sin\phi.\cos\phi(\frac{\partial\phi}{\partial z})^2 + (\alpha_2\sin^2\phi - \alpha_3\cos^2\phi)\frac{\partial v}{\partial z} + \varepsilon_0\Delta\varepsilon E^2\sin\phi.\cos\phi = \gamma_1\frac{\partial\phi}{\partial t} + I\frac{\partial^2\phi}{\partial t^2} \quad (2.52)$$

where ϕ is the deformation angle, α_2 and α_3 are the Leslie viscosity coefficients, v is the flow velocity, $\gamma_1 = (\alpha_3 - \alpha_2)$ is the rotational viscosity, I is the inertia of the LC directors, ε_0 is the free space permittivity, $\Delta\varepsilon$ is the dielectric strength and $\varepsilon_0\Delta\varepsilon E^2$ is the electric field energy density. The Erickson-Leslie equation can be applied to both parallel, perpendicular and twist alignments. Here the simplest case *i.e.* the parallel alignment has been considered. Neglecting the backflow and inertial effects in Equation 2.52, the dynamic response of parallel-aligned LC directors is described as [93]:

$$(K_{11}\cos^2\phi + K_{33}\sin^2\phi)\frac{\partial^2\phi}{\partial z^2} + (K_{33}-K_{11})\sin\phi.\cos\phi(\frac{\partial\phi}{\partial z})^2 + \varepsilon_0\Delta\varepsilon E^2\sin\phi.\cos\phi = \gamma_1\frac{\partial\phi}{\partial t} \quad (2.53)$$

Now two approaches [93] may be taken to solve the above equation i) superposition method and ii) separation of variable method.

2.3.3.1 Superposition method

In this method $\phi(z,t)$ is expanded as superposition of spatial mode with small time dependent amplitude $|C_n(t)| << 1$

$$\phi(z,t) = \sum_m C_m(t)\sin\frac{(2m+1)\pi z}{d} \quad (2.54)$$

where m stands for the number of mode. By substituting Equation 2.54 in Equation 2.53 the decay time of the m-th mode is found to be

$$\tau_m = \frac{\gamma_1 d^2}{(2m+1)^2\pi^2 K_{11}} \quad (2.55)$$

The higher order mode decays with a smaller time constant. For m=0, the lowest order spatial mode, the decay time τ_0 is often refereed as a free relaxation time

$$\tau_0 = \frac{\gamma_1 d^2}{\pi^2 K_{11}} \tag{2.56}$$

This is the expression for LC samples possessing positive dielectric anisotropy but for negative dielectric anisotropy materials, K_{11} in Equation 2.56 is replaced by K_{33}.

2.3.3.2 Separation of variable method

In this method $\phi(z,t)$ is separated into a spatial part and a time dependent part as [93]

$$\sin\phi(z,t) = h(t)\sin\phi(z) \tag{2.57}$$

where $h(t) = \sin\phi_m(t)$. ϕ_m being the maximum tilt angle of the director at z =1/2. Substituting Equation 2.57 in Equation 2.53 and simplifying the time dependent amplitude h(t) is obtained as:

$$h^2(t) = \frac{h_\infty^2}{1 + \frac{h_\infty^2 - h_0^2}{h_0^2}\exp\left(\frac{-2t}{\tau_{rise}}\right)} \tag{2.58}$$

where $h_\infty = h(t\rightarrow\infty)$ and $h_0 = h(t=0)$: the initial small fluctuation. τ_{rise} represents the rise time given by

$$\tau_{rise} = \frac{\tau_0}{\left|\left(\frac{V}{V_{th}}\right)^2 - 1\right|} \tag{2.59}$$

Similarly the decay time τ_{decay} is derived as

$$\tau_{decay} = \frac{\tau_0}{\left|\left(\frac{V_b}{V_{th}}\right)^2 - 1\right|} \tag{2.60}$$

where V_b is the bias voltage applied to the LC cell. The absolute value in the denominator indicates that this formulae is valid no matter V_b is greater or less than the threshold voltage V_{th}. For the free relaxation process it has been assumed that $V_b = 0$, which implies $\tau_{decay} = \tau_0$. Then the Equation 2.59 reduces to

$$\tau_{rise} = \frac{\tau_{decay}}{\left| \left(\frac{V}{V_{th}} \right)^2 - 1 \right|} \tag{2.61}$$

Equation 2.61 provides the direct correlation between rise time (τ_{rise}) and the decay time (τ_{decay}).

Moreover, the Erickson-Leslie equation can be greatly simplified using the small angle approximation with the following assumptions

1. Φ is small *i.e.* V is not too far above V_{th}
2. $K_{11} = K_{22} = K_{33} = K$ (one constant approximation)
3. No backflow so that v =0
4. Inertia (I) is negligible.

Under the above assumptions Equation 2.53 reduces to

$$K \frac{\partial^2 \phi}{\partial z^2} + \varepsilon_0 \Delta \varepsilon E^2 \varphi = \gamma_1 \frac{\partial \phi}{\partial t} \tag{2.62}$$

This over simplified equation also shows the same response time as those derived from Equation 2.56.

References

[1] W. Maier, A. Saupe, Eine einfache molekulare theorie des nematischen kristallinflussigen zustandes, *Z. Naturforsch* A., **13**, 564 (1958).

[2] W. Maier, A. Saupe, Eine einfache molekular-statistische theorie der nematischen kristallinflussigen phase 1, *Z. Naturforsch* A., **14**, 882 (1959).

[3] W. Maier, A. Saupe, Eine einfache molekular-statistische theorie der nematischen kristallinflussigen phase 2, *Z. Naturforsch* A., **15**, 287 (1960).

[4] I.W. Stewart, The static and dynamic continuum theory of liquid crystals: a mathematical introduction, Taylor and Francis, New York (2004).

[5] C.W. Oseen, The theory of liquid crystals, *Trans. Faraday Soc*., **29**, 883 (1933).

[6] H. Zoher, The effect of a magnetic field on the nematic state, *Trans. Faraday Soc*., **29**, 945 (1933).

[7] F.C. Frank, On the theory of liquid crystals, *Disc. Faraday Soc.*, **25**, 19 (1958).

[8] V. Fréedericksz, V. Zolina, Forces causing the orientation of an anisotropic liquid, *Trans. Faraday Soc*., **29**, 919 (1933).

[9] V. Freedericksz , V. Tsvetkov, *Phy. Z. Soviet Union*, **6**, 490 (1934).

[10] M.K. Das, A. Pramanik, B. Das, Ł. Szczuciński. R. Dąbrowski, A comparative study of the mesomorphic properties of fluoro-isothiocyanated and fluorinated terphenyl liquid crystals from birefringence, static dielectric permittivity, splay elastic constant and rotational viscosity measurements, *J. Phys. D: Appl. Phys*., **45**, 415304 (2012).

[11] A. Pramanik, B. Das, M.K. Das, K. Garbat, S. Urban, R. Dabrowski, Mesomorphic, optical, dielectric, elastic and viscous properties of multi-component isothiocyanato mixtures, *Liq. Cryst*., **40**, 149 (2013).

[12] D. Demus, L. Richter, Textures of liquid crystals, Verlag Chemie, New York (1978).

[13] I. Dierking, Textures of liquid crystals, Wiley-VCH Verlag GmbH & Co., Weinheim (2003).

[14] H. Stub, W. Perron, New method of purity determination by means of calorimetric differential thermal analysis, *Anal. Chem*., **46**, 128 (1974).

[15] P. Navard, J.M. Haudin, The height of DSC phase transition peaks application to liquid crystals, *J. Therm. Anal.*, **30**, 61 (1985).

[16] P. Narvard, R. Cox, DSC study of smectic phase transitions, *Mol. Cryst. Liq. Cryst*., **102**, 265 (1984).

[17] R. Dabrowski, K.C. Zuprynski, Advances in liquid crystal research and applications, Pergamon press, Oxford (1980).

[18] B. Das, A. Pramanik, M.K. Das, A. Bubnov, V. Hamplová, M. Kašpar, Mesomorphic and structural properties of liquid crystal possessing a chiral lactate unit, *J. Mol. Struct.*, **1013**, 119 (2012).

[19] B.R. Ratna, S Chandrasekhar, Some comments on the determination of enthalpies of liquid crystalline transitions by differential scanning calorimetry, *Mol. Cryst. Liq. Cryst.*, **162**, 157 (1988).

[20] B.K. Vainshtein, I.G. Chistyakov, Problem of modern crystallography, Nauka, Moscow (1975).

[21] A.J. Leadbetter, The molecular physics of liquid crystals, Academic Press, London (1979).

[22] A.J. Leadbetter, E.K. Norris, Distribution functions in three liquid crystals from X-ray diffraction measurements, *Mol. Phys.*, **38**, 669 (1979).

[23] L.V. Azároff, X-Ray diffraction by liquid crystals, *Mol. Cryst. Liq. Cryst.*, **60**, 73 (1980).

[24] P.S. Clegg, X-ray studies of the phases and phase transitions of liquid crystals, *Acta. Cryst. A.*, **61**, 112 (2005).

[25] H.P. Klug, L.E. Alexander, X-ray diffraction procedures, John Wiley and Sons, NewYork (1974).

[26] A.De Vries, On the calculation of the molecular cylindrical distribution function and the order parameter from x-ray diffraction data of liquid crystals, *J. Chem. Phys*., **56**, 4489 (1972).

[27] A.de Vries, X-ray photographic studies of liquid crystals i. a cybotactic nematic phase, *Mol. Cryst. Liq. Cryst.*, **10**, 219 (1970).

[28] V. Novotná, V. Hamplová, M. Kašpar, N. Podoliak, A. Bubnov, M. Glogarová, D. Nonnenmacher, F. Giesselmann, The effect of lactate unit number in compounds with azo group in the molecular core, *Liq. Cryst*., **38**, 649 (2011).

[29] A. Pramanik, M.K. Das, B. Das, V. Hamplova, M. Kašpar, A. Bubnov, Self-assembling properties of lactic acid derivative with several ester linkages in the molecular core, *Phase Transit*., **88**, 745 (2015).

[30] H.F. Gleeson, Y. Wang, S. Watson, D. Sahagun-Sanchez, J.W. Goodby, M. Hird, A. Petrenko, M.A. Osipov, On the temperature dependence of the tilt and spontaneous polarisation in high tilt antiferroelectric liquid crystals, *J. Mater. Chem.*, **14**, 1480 (2004).

[31] M. K. Das, R. Paul, Optical birefringence, density and order parameter of an ester-biphenyl mixture exhibiting an injected smectic phase, *Phase Transit.*, **46**, 185 (1994).

[32] B. Adhikari, R. Paul, Physical properties of three bicyclohexane compounds possessing smectic B phase. II: refractive index and density measurements, *Phase Transit*., **53**, 165 (1996).

[33] P.D. Roy, M.K. Das and R. Paul, Phase diagram, density and optical studies on binary mixture of a cyanobiphenyl (11OCB) and a benzoate ester (ME6.O5) showing enhanced smectic phase, *Mol. Cryst. Liq. Cryst*., **365**, 607 (2001).

[34] A.K. Zeminder, S. Paul, R. Paul, Refractive indices and orientational order parameter of five liquid crystals in nematic phase, *Mol. Cryst. Liq. Cryst.*, **61**, 191 (1980).

[35] A. Prasad, M.K. Das, Refractive index and orientational order parameter of a polar–polar binary system showing induced smectic A_d and re-entrant nematic phases, *Phase Transit.*, **83**, 1072 (2010).

[36] G. Sarkar, M.K. Das, R. Paul, B. Das, W. Weissflog, Comparison of the orientational order parameters determined from X-ray diffraction and ^{13}C NMR studies of a hockey stick-shaped compound, *Phase Transit*., **82**, 433 (2009).

[37] A. Prasad, M.K. Das, Optical birefringence studies of a binary mixture with the nematic–smecticA_d-re-entrant nematic phase sequence, *J. Phys. Condens. Matter*, **22**, 195106 (2010).

[38] S.K. Sarkar, M.K. Das, Critical behaviour at the nematic–smectic A phase transition in a binary mixture showing induced nematic phase, *RSC Adv*., **4**, 19861 (2014).

[39] S. K. Sarkar, P.C. Barman, M.K. Das, Optical birefringence and its critical behavior in the vicinity of nematic–smectic A phase transition in a binary mixture, *Physica B*, **446**, 80 (2014).

[40] S.K. Sarkar, M.K. Das, Critical behavior of optical birefringence at the nematic–smectic A phase transition in a binary liquid crystal system, *J. Mol. Liq.*, **199**, 415 (2014).

[41] A. Saipa, F. Giesselmann, A high resolution temperature scanning technique for optical studies of liquid crystal phase transitions. *Liq. Cryst.*, **29**, 347 (2002).

[42] T. Scharf, Polarized light in liquid crystals and polymers, NJ:Wiley, Hoboken (2007).

[43] M.F. Vuks, Determination of optical anisotropy of aromatic molecules from double refraction of crystals, *Opt. Spectros.*, **20**, 361 (1966).

[44] H.E. Neugebauer, Clausius-Mosotti equation for certain types of anisotropic crystals, *Canad. J. Phys.*, **32**, 1 (1954).

[45] I. Haller, Thermodynamic and static properties of liquid crystals, *Prog. Solid State Chem.*, **10**, 103 (1975).

[46] W.H. de Jue, Physical properties of liquid crystalline materials, Gordon and Breach, London (1980).

[47] W. Kuczynski, B. Zywucki, J. Malecki, Determination of orientational order parameter in various liquid-crystalline phases, *Mol. Cryst. Liq. Cryst.*, **381**, 1 (2002).

[48] A. Prasad, M.K. Das, Static dielectric properties of two nematogenic compounds and their binary mixtures showing induced smectic A_d and re-entrant nematic phases, *Phys. Scr.*, **84**, 015603 (2011).

[49] P. Dasgupta, B. Das, M.K. Das, Dielectric and visco-elastic properties of laterally fluorinated liquid crystal single compounds and their mixture, *Liq. Cryst.*, **39**, 1297 (2012).

[50] A. Chakraborty, M.K. Das, B. Das, U. Baumeister, W Weissflog, Optical, dielectric and visco-elastic properties of a few hockey stick-shaped liquid crystals with a lateral methyl group, *J. Mater. Chem. C*, **1**, 7418 (2013).

[51] S. Basak, P. Dasgupta, B. Das, M.K. Das, R. Dabrowski, Dielectric permittivity and viscoelastic measurements of two tricomponent mixtures consisting of laterally fluorinated terphenyl derivatives, *Acta. Phys. Pol. A*, **123**, 714 (2013).

[52] S.K. Sarkar, M.K. Das, Critical behavior of dielectric permittivity in the vicinity of nematic–isotropic and smectic–nematic phase transitions in smectogenic binary mixtures, *Fluid Phase Equilib.*, **365**, 41 (2014).

[53] S.K. Sarkar, M.K. Das, Dielectric studies and critical behaviour in the vicinity of nematic–isotropic phase transition of a smectogenic binary mixture showing induced nematic phase, *Liq. Cryst.*, **41**, 1410 (2014).

[54] E.A. Guggenheim, A proposed simplification in the procedure for computing electric dipole moments, *Trans. Faraday Soc.*, **45**, 714 (1949).

[55] A.G. Gilani, A. Ramjkesh, M.S. Beevers, Dipole moments of flourobenzene and its mesogenic derivative in 1,4-dixone and 1-butanol solutions, *J. Solutions Chem.*, **38**, 557 (2009).

[56] D.G. McDonnell, E.P. Raynes, R.A. Smith, Dipole moments and dielectric properties of fluorine substituted nematic liquid crystals, *Liq. Cryst.*, **6**, 515 (1989).

[57] MOPAC. [Internet]. USA: Stewart computational chemistry, Colorado Springs. 2009 [cited 2008]. Available from: http://OpenMOPAC.net.

[58] M. Heng, S. Rui-Zhi, L. Zhen-Xin, Mechanical model study of relationship of molecular configuration and multiphase in liquid crystal materials, *Chin. Phys. B.*, **15**, 1009 (2006).

[59] H. Gruler, T.J. Schiffer, G. Meier, Elastic constants of nematic liquid crystals, *Z. Natureforsh*., **27A**, 966 (1972).

[60] L. Csillag, I. Jánossy, V.F. Kitaeva, N. Kroó, N. Sobolev, A.S. Zolotko, Laser induced reorientation of nematic liquid crystals, *Mol. Cryst. Liq. Cryst.*, **78**, 173 (1981).

[61] A. Chakraborty, M.K. Das, B. Das, A. Lehmann, C. Tschierske, Rotational viscosity measurements of bent-core nematogens, *Soft Matter*, **9**, 4273 (2013).

[62] A. Prasad, M.K. Das, Determination of elastic constants of a binary system (7CPB+9.CN) showing nematic, induced smectic A_d and re-entrant nematic phases, *Liq. Cryst.*, **41**, 1261 (2014).

[63] S.T. Wu, C.S. Wu, Experimental confirmation of the Osipov-Terentjev theory on the viscosity of nematic liquid crystals, *Phys. Rev. A*, **42**, 2219 (1990).

[64] M.L. Dark, M.H. Moore, D.K. Shenoy, R. Shashidhar, Rotational viscosity and molecular structure of nematic liquid crystals, *Liq. Cryst.*, **33**, 67 (2006).

[65] M.K. Das, A. Prasad, Rotational viscosity measurement of a binary mixture showing both induced smectic and re-entrant nematic phases, Mol. Cryst. Liq. Cryst., **540**, 162 (2011).

[66] S.T. Wu, U. Efron, L.D. Hess, Birefringence measurements of liquid crystals, *Appl. Opt.*, **23**, 3911 (1984).

[67] S.T. Wu, C.S. Wu, M. Warenghem, M. Ismaili, Refractive index dispersions of liquid crystals, *Opt. Eng*., **32**, 1775 (1993).

[68] P. Sathyanarayana, T.A. Kumar, V.S.S. Sastry, M. Mathews, Q. Li, H. Takezoe, S. Dhara, Rotational viscosity of a bent-core nematic liquid crystal *Appl. Phys. Exp.*, **3**, 091702 (2010).

[69] S.T. Wu, A.M. Lackner, U. Efron, Optimal operation temperature of liquid crystal modulators, *Appl. Opt*., **26**, 3441 (1987).

[70] A. Parish, S. Gauza, S.T. Wu, J. Dziaduszek, R. Dabrowski, New fluorinated terphenyl isothiocyanate liquid crystals, *Liq. Cryst.*, **35**, 79 (2008).

[71] M.J. Bradshaw, D.G. McDonnell, E.P. Rayens, Physical properties of nematic materials containing different ring systems, *Mol. Cryst. Liq. Cryst.*, **70**, 289 (1981).

[72] J. Nehring, A. Saupe, Calculation of the elastic constants of nematic liquid crystals, *J. Chem. Phys.*, **56**, 5527 (1972).

[73] K. Miyasato, S. Abe, H. Takezoe, A. Fukuda, E. Kuze, Direct method with triangular waves for measuring spontaneous polarization in ferroelectric liquid crystals, *Jpn. J Appl. Phys.*, **22**, L661 (1983).

[74] A. Pramanik, M.K. Das, B. Das, M. Żurowska, R. Dabrowski, Electro-optical properties of a new series of fluorinated antiferroelectric orthoconic liquid crystalline esters, Liq. Cryst., **42**, 412 (2015).

[75] S.S. Bawa, A.M. Biradar, K. Saxena, S. Chandra, Direct pulse technique for spontaneous polarization dynamics and molecular reorientation processes in ferroelectric liquid crystals, *Rev. Sci. Instrum.*, **59**, 2023 (1988).

[76] M. Hird, Flourinated liquid crystals properties and applications, *Chem. Soc. Rev.*, **36**, 2070 (2007).

[77] M. Glogarova, H. Sverenyak, A. Fukuda, H. Takezoe, Electrooptic properties of chiral smectic liquid crystals with a dipolar order, *Liq. Cryst.*, **14**, 463 (1993).

[78] K. Furukawa, K. Terashima, M. Ichihashi, S. Saitoh, K. Miyazawa, T. Inukai, Substituent ortho to the chiral tail group-a study of a factor

determining the magnitude of spontaneous polarization. *Ferroelectrics*, **85**, 451 (1988).

[79] V.M. Vaksman, Y.U.P. Panarin, Measurement of ferroelectric liquid crystal parameter, *Mol. Mats.*, **1**, 147 (1992).

[80] L.M. Blinov, V.G. Chigrinov, Electro-optical effects in liquid crystal materials, Springer-Verlag, New York (1994).

[81] A.I. Allagulov, S.A. Pikin, V.G. Chigrinov, Bistable and monostable polarized states of a liquid-crystalline ferroelectric in an electric field, *Liq. Cryst.*, **5**, 1099 (1989).

[82] A.K. Misra, A.K. Srivastava, J.P. Sukla, R. Manohar, Dielectric and electro-optical parameters of two ferroelectric liquid crystals: a comparative study, *Phys. Scr.*, **78**, 065602 (2008).

[83] J.F. Lyuu, C.C. Chen, J.Y. Lee, The anchoring energy coefficient of dye guest-host ferroelectric liquid crystals, *Mol. Cryst. Liq. Cryst.*, **329**, 99 (1999).

[84] R. Manohar, S.P. Yadav, K.K. Pandey, A.K. Srivastava, A.K. Misra, Comparative study of dielectric and electro-optical properties of pure and polymer ferroelectric liquid crystal composites, *J. Polym. Res.*, **18**, 435 (2011).

[85] R.L. Humphries, P.G. James, G.R. Luckhurst, Molecular field treatment of nematic liquid crystals, *J. Chem. Soc., Faraday Trans. II*, **68**, 1031 (1972).

[86] P.G. de Gennes, The physics of liquid crystal, Clarendon Press, Oxford (1974).

[87] S. Chandrasekhar, Liquid crystals, Cambridge University Press, Cambridge (1977).

[88] G.R. Luckhurst, G.W. Gray (Editors), The molecular physics of liquid crystals, Academic Press, London (1979).

[89] M. Kleman, Points, lines and walls, Wiley, New York (1983).

[90] F.M. Leslie, Handbook of liquid crystals, Wiley-VCH, New York (1998).

[91] J.L. Erickson, Conservation laws for liquid crystals, *Trans. Soc. Rheol.*, **5**, 23 (1961).

[92] F.M. Leslie, Some constitutive equations for liquid crystals, *Arch. Ration. Mech. Anal.*, **28**, 265 (1968).

[93] I.C. Khoo, S.T. Wu, Optics and nonlinear optics of liquid crystals, World Scientific Publishing, Singapore (1993).